



PERGAMON

Journal of Geodynamics 35 (2003) 59–81

JOURNAL OF
GEODYNAMICS

www.elsevier.com/locate/jog

The August–December 2000 earthquake swarm in NW Bohemia: the first results based on automatic processing of seismograms

Tomáš Fischer*

Geophysical Institute, Acad. Sci. Czech Republic, Prague, Czech Republic

Abstract

Main features of the August–December 2000 earthquake swarm which occurred in the major focal area of the North-West Bohemia / Vogtland swarm region are presented. Seismograms from four stations of WEBNET were automatically processed to get arrival times, first motion amplitudes and hypocentre coordinates of a representative set of events. Altogether 7017 microearthquakes in the magnitude range of $M_L=0-3.3$ were identified. It is shown the decay of activity of individual swarm phases followed the modified Omori law, which points to a partial similarity with aftershock sequences of tectonic earthquakes. The space-time distribution of a subset of 2913 events with low location residuals shows a strong space clustering of the earthquake hypocentres and their pronounced migration between individual swarm phases. Most of the activity took place along an elliptical, nearly vertically dipping, 6 km long N-S oriented fault plane in depths ranging from 10.5 to 6.5 km. The P and T axes were estimated by FOCMEC for the 782 strong events and three groups of earthquakes with similar faulting type were distinguished. In contrast to the normal and strike-slip faulting events that created the prevailing portion of the swarm and were distributed uniformly within the focal area, the reverse events were clustered in time and space.

© 2002 Elsevier Science Ltd. All rights reserved.

1. Introduction

The northwestern part of the Bohemian massif, often referred to as the NW-Bohemia/Vogtland earthquake swarm region, covers the Czech–German border area of about 6000 km² (Fig. 1). It is typical by the recurrence of intraplate seismic swarms with maximum magnitudes of up to 4.5.

* Corresponding author. Fax: +42-2-6710-3365.

E-mail address: tomas@ig.cas.cz (T. Fischer).

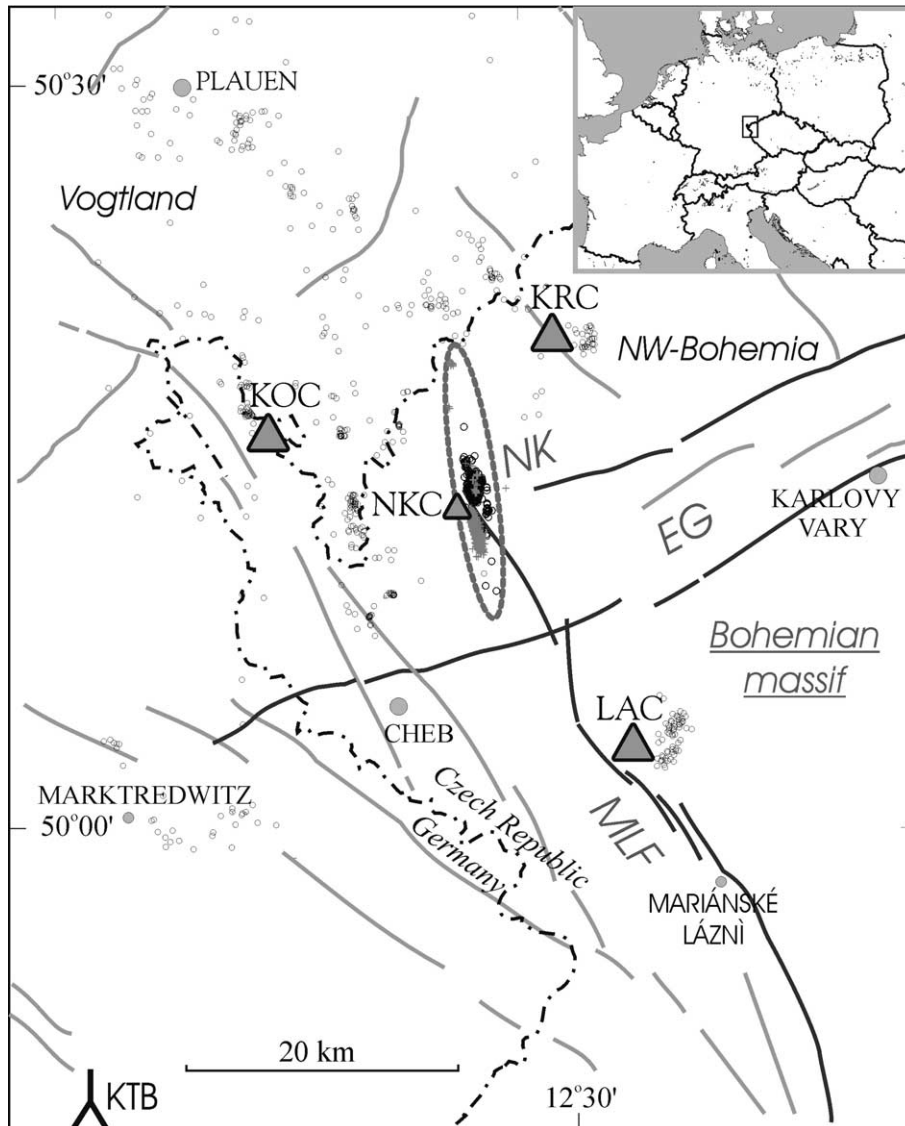


Fig. 1. The NW-Bohemia/Vogtland earthquake swarm region. The WEBNET stations, which provided data for this study are denoted by full triangles. Circles denote epicentres of microearthquakes in the period 1991–1999, the swarm 2000 epicentres are marked by grey crosses. Ellipse delineates the main swarm area of Nový Kostel (NK), lines indicate the faults. Fault systems are denoted as *MLF* (Mariánské Lázně fault) and *EG* (Eger rift).

The swarm seismicity strongly clusters in space and time, altogether 10 swarms with maximum magnitudes $M_{Lmax} > 2$ appeared in the whole region within the past 15 years (Neunhöfer, 2000). Among them, the M_{Lmax} 4.5 swarm of 1985/86, M_{Lmax} 2.0 swarm of January 1992, M_{Lmax} 2.5 swarm of December 1994 and M_{Lmax} 3.0 swarm of January 1997, occurred in the Nový Kostel area (denoted *NK* in Fig. 1).

Three principal tectonic units—the Saxothuringian, Moldanubian, and Teplá-Barrandean Unit—make contact there. The area is further intersected by an ENE-WSW striking neotectonic structure, the Eger Graben (*EG*), dominant from a geodynamics point of view. The movements along the *EG* are predominantly vertical; no geological evidence for larger horizontal displacements exists (Dudek, 1987). The Mariánské Lázně fault (*MLF*), striking NNW-SSE, is probably terminated in a conjunction with the *EG* (Fig. 1). Until recently, the *MLF* was considered to be dominant in the region under study. The tectonosedimentary evolution of the area is given in Špičáková et al. (2000).

Other geophysical and geological phenomena typical for the western part of the Bohemian Massif are negative gravity anomalies (Švancara et al., 2000), vertical motions of the upper crust in the seismically active area (Mrlina, 2000), increased heat flow (Čermák et al., 1996), quaternary volcanism active till the Holocene (Wagner et al., 1998), abundant occurrence of juvenile carbon-dioxide waters, rich CO₂ emissions, anomalies of mantle-derived He and geothermal springs (Heinicke and Koch, 2000; Weise et al., 2001).

From the observational viewpoint, the earthquake swarms differ from typical mainshock-after-shock sequences mainly by a missing dominant mainshock. No regular decrease of swarm activity is observed, and the *b*-value of their magnitude–frequency distribution is larger than that of aftershock sequences at plate boundaries (Lay and Wallace, 1995). Anomalous characteristics of swarms are usually attributed to fluids activity (Hill, 1977; Yamashita, 1999), or to a heterogeneous stress system (Lay and Wallace, 1995). New results from spring-block models show that the temporal clustering and magnitude–frequency distribution of swarms can be simulated without the presence of active fluids by increasing the postseismic response of the viscoelastic models (Hainzl, 2002).

The swarms of 1985/86 and of January 1997 were studied in detail by a number of authors. During the 1985/86 swarm new digital seismic stations were deployed in the area. This brought a great deal of new knowledge about the origin and behaviour of the NW-Bohemia/Vogtland earthquake swarms. The works focused mainly on hypocentre localisation (Horálek et al., 1987; Šílený, 1987), seismo-statistics, macroseismic investigations, and focal mechanisms (Grosser et al., 1987; Antonini, 1988; Zahradník et al., 1989). The swarm of January 1997 was the first well recorded medium-size swarm which enabled us to carry out a precise investigations including both refined event localisation (Fischer and Horálek, 2000) and focal mechanism determination (Dahm et al., 2000; Horálek et al., 2000b; Vavryčuk, 2001). These studies first indicated the presence of an isotropic component in the moment tensors of some events of the January 1997 swarm and inferred that this may be an indication of fluid activity during the faulting process. At the south-western edge of the area of interest, the KTB superdeep borehole is located, which had reached a final depth of 9101 m. By the fluid-injection experiments several hundreds of micro-earthquakes were induced in the 9 km depth, which is similar to the depth of the swarm earthquakes. Although injection-induced events are supposed to exhibit dilatational component, the moment tensors displayed prevailing double-couple sources (Jost et al., 1998).

In the period from August to December 2000, more than 10 000 microearthquakes in the Nový Kostel focal zone with magnitudes up to 3.3 were recorded by local seismic networks operating in the area. With respect to the magnitude range and to the duration of seismic activity this swarm represents one of the most outstanding NW-Bohemia/Vogtland earthquake swarm episodes of the 20th century and has been the most intensive swarm since the M_L 4.5 swarm of 1985/86. The macroseismic effects of the largest shocks were felt in an area of up to 50 km in diameter. The

swarm 2000 lasted from August 28 until December 26, 2000 and consisted of altogether nine sub-swarm episodes (swarm phases), each of them lasting for several days. This successive way of seismic energy release is typical for most of the NW-Bohemia/Vogtland earthquake swarms, however the swarm 2000 was unique with respect to the number of swarm phases and their well pronounced character.

All the local seismic stations operating in the area recorded the events of the 2000 swarm. This paper deals with the data recorded by the WEBNET local seismic network (Horálek et al., 2000a). The enormous amount of waveform data was a motivation for developing a procedure suitable for automatic processing of records of local swarm earthquakes occurring in this area. This procedure has been described in a previous paper (Fischer, 2002). In this paper I present (i) the basic space-time pattern of the whole 2000 swarm based on automatic processing and (ii) classification of the swarm events on the basis of automatically picked onset amplitudes.

2. Data

The West-Bohemian local seismic network WEBNET (see Fig. 1) is operated in a coincidence trigger mode using a sampling frequency of 250 Hz. During the swarm 2000 it was formed by two telemetric subnets A and B, by two permanent and three temporary autonomous stations. The stations of Subnet A (NKC, KRC, KOC and LAC) are deployed near individual epicentral zones of the area and provide the high sensitivity of the network as a whole. They were equipped with 2-s SM-3 seismometers and a Lennartz PCM 5800 data acquisition system. The continuous data were transmitted to the data centre where 12 data channels were mixed together and event files were created in a synchronous mode using STA/LTA detector. Each of the event files contained three-component records for all four stations of Subnet A. A homogeneous data set comprising equal event-station pairs was thus created. The other parts of WEBNET did not provide equally homogeneous data because of frequent recording outages. The event files from both subnets were stored on a PC disk in the remote data centre next to the epicentral area and transmitted via the Internet to the data processing centre at the Geophysical Institute in Prague.

The available data set covered the period from August 28, 2000 to January 31, 2001. Only Subnet A stations were used for automatic processing due to following reasons: (1) they provided data covering the whole swarm duration period with a minimum of recording outages and (2) the data format comprising equal event-station pairs allowed for a straightforward application and unattended operation of the automatic procedure.

The final data set used for automatic processing comprised more than 6000 event files. Most of them contained waveforms of numerous earthquakes; the first estimate of the total number of swarm earthquakes was more than 10 000. The epicentral distances ranged from several hundred of meters at NKC to 20 km at LAC, see Table 1.

3. Method

The records of the earthquakes of the August–December 2000 swarm used in this study were processed automatically by the new method described in Fischer (2002).

Table 1
WEBNET stations used for automatic processing

Station	Latitude N (°)	Longitude E (°)	Elevation (m)	Mean epicentral distance
NKC	50.2331	12.4479	564	0
KRC	50.3316	12.5304	560	13
KOC	50.2652	12.2336	575	14
LAC	50.0508	12.6250	838	20

3.1. Phase picking

In order to identify records of individual events in the seismic traces, the automatic method takes advantage of the nearly horizontal polarisation of S-waves, which is typical for the waveforms of local earthquakes in this area (see Fig. 2). The phase picker is applied in two steps: first, S-wave groups are identified in the points of local maxima of horizontal polarisation. Then the peaks of vertical polarisation preceding the S-wave groups, which represent the corresponding P-wave groups, are searched for. The times of maxima of P- and S-wave groups are then used as starting points for an accurate P- and S-arrival time search. The closest station to the swarm area (NKC) is used as master, and the phase search at the remaining stations is governed by P- and S-phases identified at the master station. Each combination of the candidate P- and S-phases is checked by preliminary hypocentre location. Due to the use of a priori information on the approximate position of the event hypocentres the method is partially capable to pick pairs of mixed P- and S- phases of rapid sequences of multiple events, which are common in earthquake swarms. An example of a mixed phase situation is illustrated in Fig. 3 where waveforms and automatic picks of two interfering events of magnitudes 0.4 and 0.7 are shown. As follows from the fig. for both events the phases were associated correctly and the phase picks are quite accurate. The method is not sensitive to regional and quarry blast events thanks to the combination of

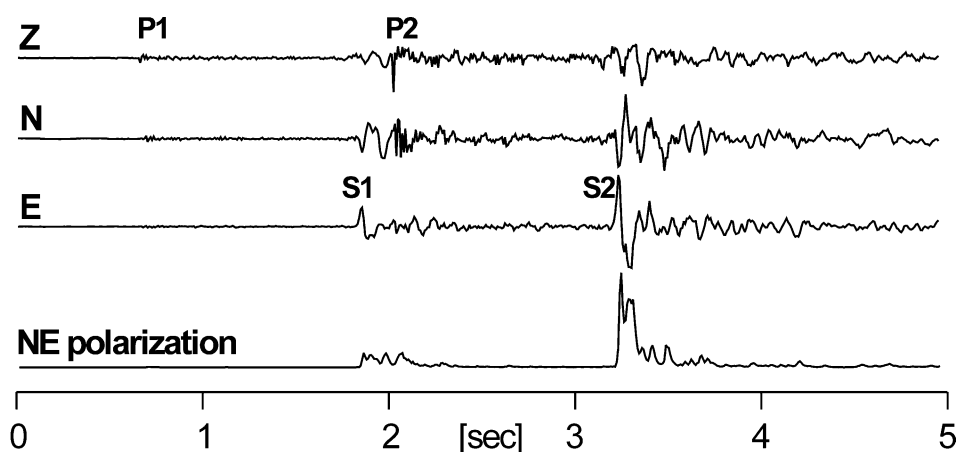


Fig. 2. A record of two swarm 2000 events (3-Sep-00, 21:53:10, $M_L=0.4$ and $M_L=0.7$, station NKC) with overlapping waveforms. The bottom trace shows the maximum eigenvalue of the signal covariance matrix in the horizontal plane (Magotra et al., 1987), which is used as the S-wave detector. P- and S-phases of individual events are indicated.

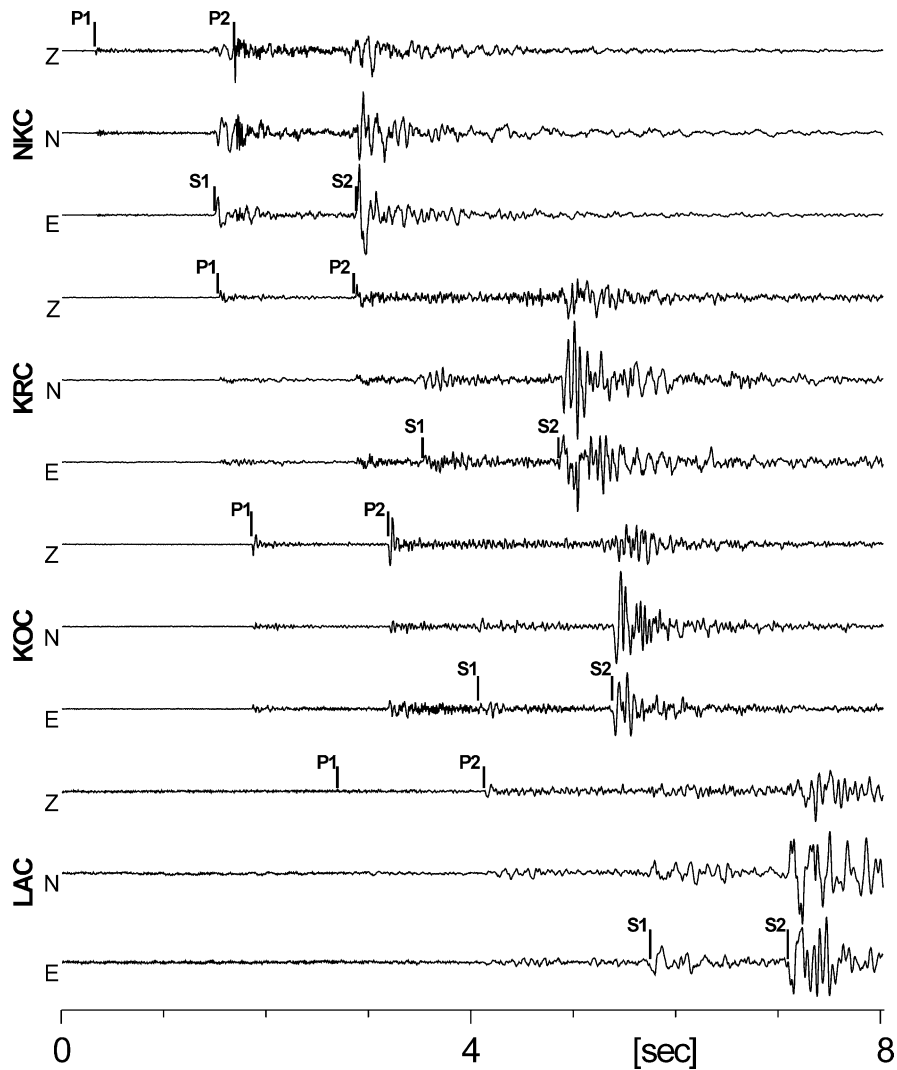


Fig. 3. An example of a successful automatic pick of two mixed events from Fig. 2. Recordings at four WEBNET stations, which were used for automatic processing, are shown. The position of automatically obtained P- and S-wave picks is indicated.

two criteria: first, the polarisation pattern of waveforms of these spurious events is fairly different from that of local earthquakes; second, if the polarisation detector misidentifies the record as waveform of a local earthquake, the strict criteria of a priori known approximate hypocentre position excludes the event from further processing.

The automatic picks obtained within this study are being used as a hint for manual picking of the 2000 swarm events. From 14 100 onset times manually picked during the evaluation test, 9000 were found by the automatic procedure. Following the report of experienced interpreters (Boušková et al., 2002), most of the time readings are surprisingly accurate: more than 95% of the picks show timing errors less than ± 6 and ± 12 ms (± 1.5 and ± 3 samples) for P and S waves,

respectively. Gross errors occur only exceptionally in cases of very weak ($M_L < 0$) events and sometimes in situations of interfering (mixed phase) events.

3.2. Localisation

Simultaneous location was carried out by grid search using a homogeneous velocity model. The parameters of the model are based on the study of Janský et al. (2000) in which a set of suitable homogeneous and 1-D velocity models, depending on the epicentre area and seismic stations used for the inversion, is given. A homogeneous model was accepted as a suitable simplification for the automatic procedure because the results of Janský et al. (2000) showed that a homogeneous model is a sufficient approximation for location of events inside WEBNET. Because we used only four of the ten stations employed in Janský's study, a slightly different velocity model $v_P = 5950$ m/s and $v_P/v_S = 1.71$ was chosen, which resulted in a minimum of the misfit function.

To suppress the location error caused by station residuals, which takes effect in the case of missing arrival times at individual stations, only the events with all eight arrival time readings were processed. The location error, resulting mainly from inaccuracy in P- and S-arrival time picking, was estimated as the distance from the hypocentre in which the location residual function reaches the level $S_0(\sigma_{TP}, \sigma_{TS})$ derived by the error propagation method from the arrival time errors σ_{TP} and σ_{TS} as

$$S_0 = \sqrt{\frac{2}{n}(\sigma_{TP}^4 + \sigma_{TS}^4)} \quad (1)$$

The automatic method was tested by Fischer (2002) on the data of the 1997 swarm, which occurred in the same epicentral area, by comparing the swarm catalogues obtained manually and automatically. It was shown that the events with small residuals S_0 of automatic location display also low location errors in terms of the difference between the automatically and manually obtained hypocentre coordinates.

4. Results

In total, 7017 earthquakes occurring in the Nový Kostel area within the investigated period were identified by the automatic method. Only the events with P- and S-wave readings on all four stations were accepted for further processing. The following parameters were obtained for each event:

- P- and S-wave arrival times
- P- and SH-wave onset polarities and amplitudes
- Origin time t_0 and hypocentre coordinates x_0, y_0, z_0 . The location error was estimated using (1) by setting the uncertainty of automatic arrival time picks to a more pessimistic estimate of ± 8 ms for P- and ± 16 ms for S-waves. The error of automatic localisations of the whole data set approached maximum values of ± 110 m in E-W, ± 90 m in N-S, and ± 190 m in vertical coordinates.

- Local magnitude estimate M_L . For magnitude determination the formula derived for WEBNET stations (Horálek et al., 2000a) was used.
- Location residuals sum S_0 resulting from the arrival times reading error.

The resulting catalogue was investigated with respect to the location residuals and the magnitude–frequency distribution in order to evaluate the quality of the data and their magnitude range.

For the swarm of 1997 the distance between the automatic and manual locations was less than 80 m in each coordinate for events with $S_0 < \text{six samples}$ (24 ms). From Fig. 4 follows that the location residual was less than 6 samples also for most events of the swarm 2000. This group comprises 100% of events with $M_L > 3.0$, 92% of $M_L > 2.0$ events, and 65% (4527) of all located events. As expected, inaccurate phase picking is more frequent for weak events. Following Fig. 5 where the magnitude–frequency distributions $N(M_L)$ of all events and of accurately located events are shown, we consider the catalogue to be complete down to the magnitude of 0.4. Hence we limited further processing to $M_L > 0.4$ earthquakes. Additional condition of low location residuals ($S_0 < 6$ samples) was applied for the investigation of the space–time distribution and for estimating the focal mechanisms, which are more sensitive to phase picking and location errors.

4.1. History of the swarm

4.1.1. Swarm phases

The history of the swarm 2000, based on automatic event recognition, is shown in Fig. 6. Nine swarm phases with the maximum magnitudes exceeding the value of 2.5, and five of them with the strongest event magnitudes larger than 3.0, were distinguished. The swarm phases were typical by an abrupt increase of seismic activity gradually decaying until the opening of the next swarm

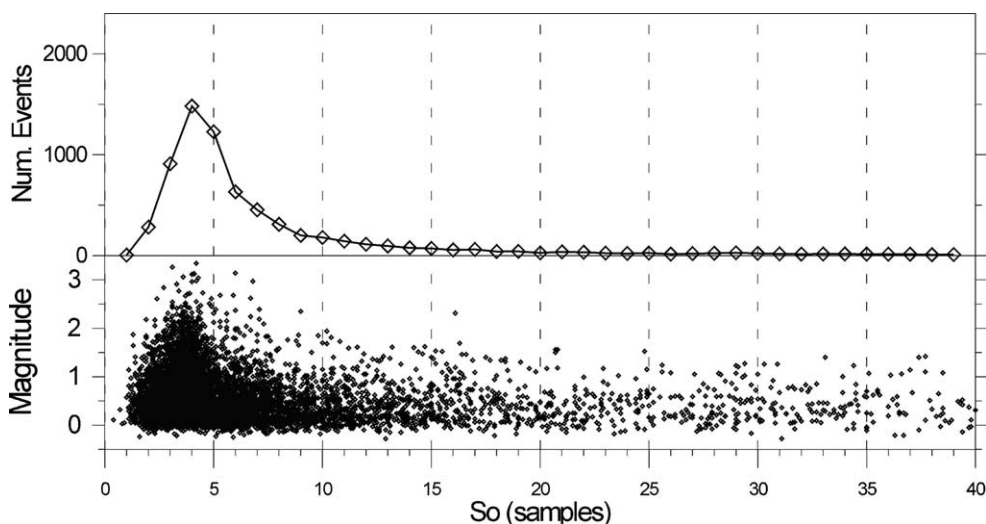


Fig. 4. Distribution of the location residual S_0 . Top: number of events with S_0 below the upper bin limit. Bottom: Dependence of event magnitudes on S_0 .

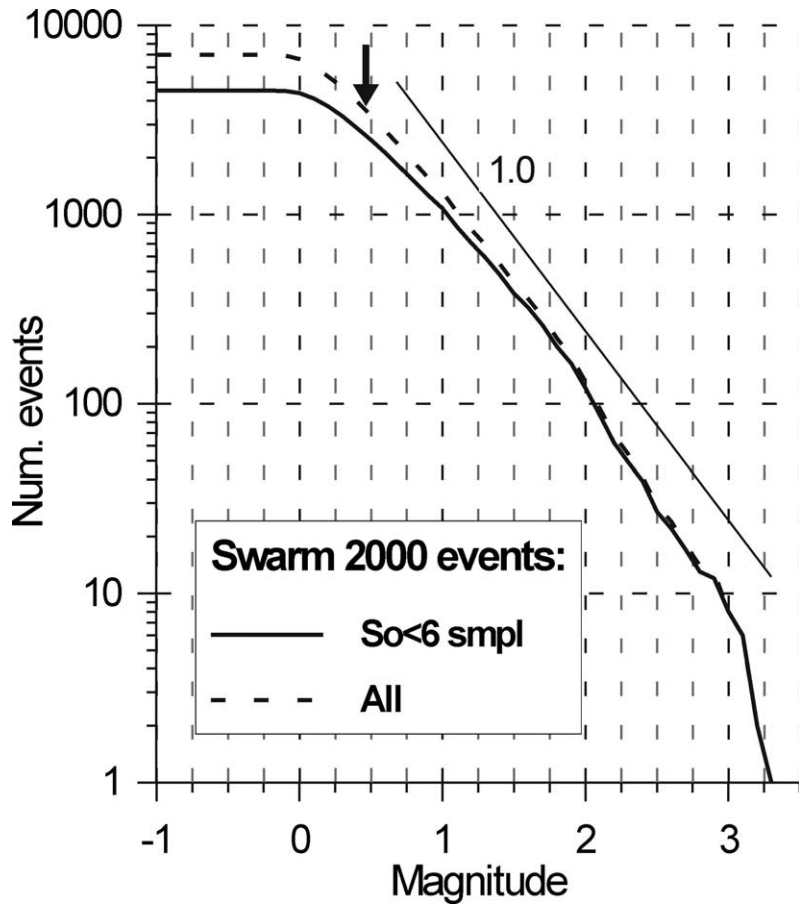


Fig. 5. Magnitude–frequency distribution of the swarm 2000. Dashed line: all located events; full line: accurately located events. Arrow: lower magnitude limit for further processing. The slope corresponding to $b = 1$ is indicated.

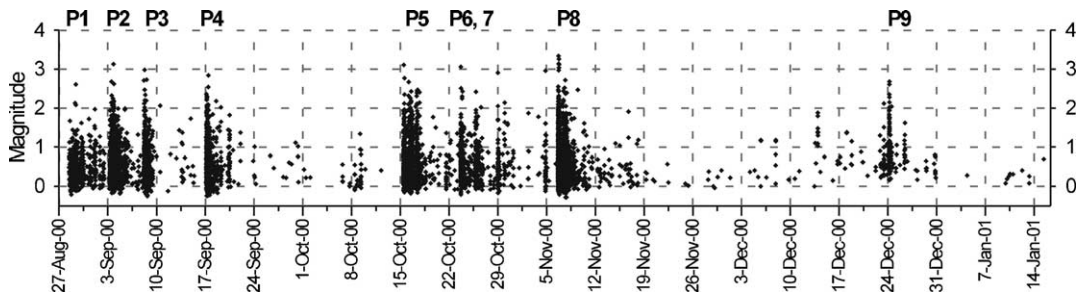


Fig. 6. History of the swarm 2000—magnitude scatter plot. P1–P9 indicate the swarm phase numbers.

phase. In this way, the swarm phases resemble the classical aftershock sequences observed at plate boundaries, which obey the modified Omori’s law (Utsu, 1961). The culmination period of each swarm phase lasted for the first dozens of hours, whereas the relaxation period duration, which was characteristic by the occurrence of weak $M_L < 1.0$ events, varied from several days up to 1 month.

To study the swarm evolution process and with the aim to reveal characteristic features of individual swarm phases, the waiting time τ of subsequent events was investigated. It expresses the time delay between the occurrences of consecutive earthquakes of size above a selected cutoff, displaying the frequency of subsequent events. The distribution of waiting times is usually used to study the clustering and periodicity of earthquake occurrence (Kagan and Jackson, 1991; Hainzl et al., 2000). In this paper, we investigate the temporal dependence of τ to study the development of the swarm process. Accelerating of the activity in the beginning of a swarm phase is displayed in a rapid decrease of τ , whereas τ increases at the end of the swarm phase culmination period and in the course of the relaxation period. Hence the minimum of τ corresponds to the culmination period of a swarm phase.

To determine the duration of the culmination period quantitatively, the onset and the end of the waiting times minimum were identified. To this purpose a classical STA/LTA detector was applied on the time series of the waiting time data. The onset of each swarm phase was identified in the point where the STA/LTA ratio fell below a predefined value, whereas the end of the swarm phase was declared after the STA value of the waiting time exceeded a fixed threshold. The resulting duration of individual culmination periods is given in Table 2. Also the overall average value and minimum 1-h average of waiting times are displayed for each swarm phase. The results show, in accordance with Fig. 7, that the waiting times for events with $M_L > 0.4$ varied substantially between particular phases. The first swarm phase was the “slowest” one—its average waiting time is 3–4 times longer than the average waiting time of further swarm phases, and its minimum one-hour average of waiting times is 10 times larger than that of the phase 8 which was the “fastest” one.

4.1.2. Decay of activity

None of the swarm phases shows a simple picture of generation of new events, always the history is more complex. The plot of cumulative number of events on the top of Fig. 7 shows that

Table 2
Parameters of phases of the swarm 2000

No.	Swarm phase onset	M_{Lmax}	Culmination period			Relaxation period			
			D [h]	$\langle \tau \rangle$ [s]	$min(\tau)$ [s]	D [h]	P	e_p	R
1	Aug 28, 16:26	2.6	67	1270	188	74	–	–	–
2	Sep 03, 13:01	3.1	75	336	29	68	0.54	0.088	0.589
3	Sep 08, 10:28	3.0	42	457	78	210	1.08	0.130	0.607
4	Sep 17, 04:36	2.8	63	569	31	283	1.18	0.082	0.695
5	Oct 15, 16:46	3.1	89	470	44	100	1.91	0.180	0.785
6	Oct 23, 21:29	3.1	47	1019	52	5	–	–	–
7	Oct 26, 01:30	2.9	41	1560	152	200	–	–	–
8	Nov 06, 21:03	3.3	78	269	18	669	1.26	0.100	0.782
9	Dec 24, 09:58	2.7	23	565	55	972	0.95	0.061	0.857

D : duration of culmination period in hours; $\langle \tau \rangle$: average waiting time; $min(\tau)$: minimum 1-h average of waiting time; P : P -value of the modified Omori relation; e_p : standard error of P value; R : regression coefficient. The relaxation periods of swarm phases 1, 6, and 7 were not investigated due to their short duration and significant background seismicity.

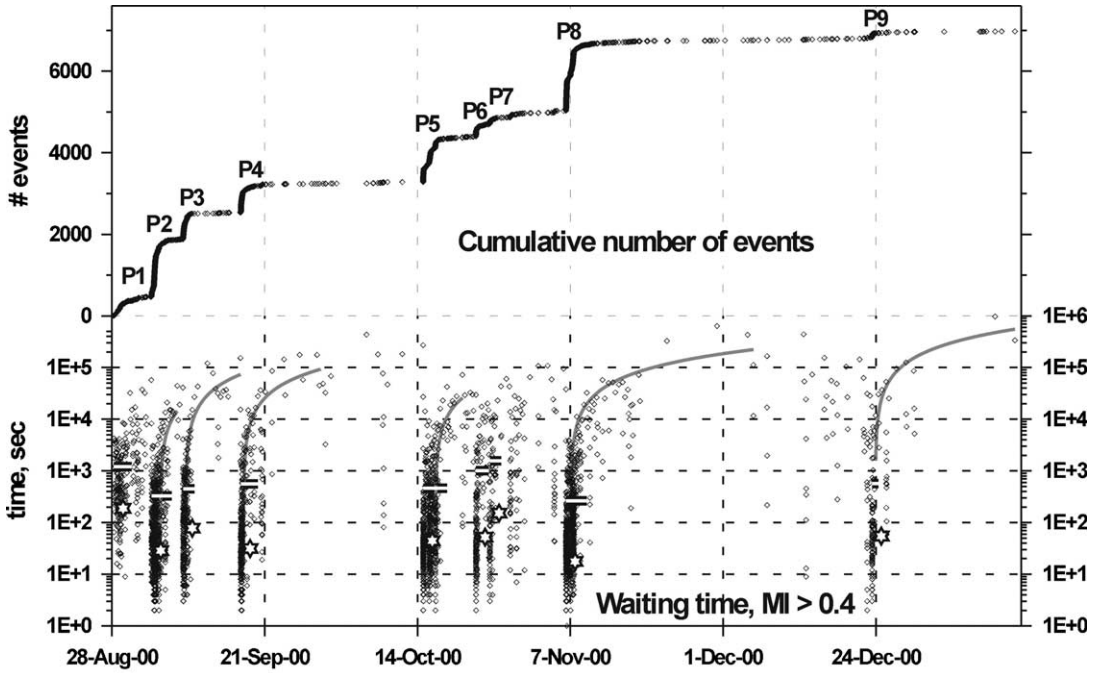


Fig. 7. History of the swarm 2000. Top: cumulative number of events. Bottom: waiting time (time delay between occurrence time of consecutive events above the magnitude cutoff). Horizontal bars: average waiting times of culmination period of each swarm phase; their length shows the swarm phase duration. Asterisk: minimum 1-h average of waiting time. Curves: approximation of Omori's law for the relaxation periods of swarm phases. P1–P9 indicate the swarm phase numbers.

within most swarm phases the rupture process started rapidly and slowed down after dozens of minutes, being accelerated again after some time. The most complex was probably phase P7—it started on Oct. 26 by a dense $M_L=2.4$ cluster, nevertheless two later $M_L=2.9$ sparse clusters appeared on Oct. 29 and Nov. 5. The relaxation periods display a clearly monotonous increase of waiting times; their values reach at least 10 000 s in-between each swarm phase. In this respect the swarm phases resemble aftershock sequences for which the modified Omori law $n(t) = K (t + c)^{-p}$ (Utsu, 1961), is generally valid. Here, $n(t)$ is the frequency of aftershocks per unit time interval, t is the lapse time from the mainshock and K , c and p are parameters. To test the hypothesis of similarity of swarm phases to aftershock sequences, we applied the modified Omori formula to the waiting time τ , which is an inverse of $n(t)$. By rearranging the formula for τ , we get

$$\tau = 1/K(t + c)^p, \tag{2}$$

For the present study the use of the waiting time instead of the frequency of events is more suitable because the time scale of a swarm is much shorter than that of an aftershock sequence, and also the number of shocks in a swarm sequence is lower. When processing aftershock sequences, the lapse time t is measured from the occurrence of the mainshock. In the case of swarms there is no clear mainshock, and most phases of the 2000 swarm contain multiple shock

sequences. It therefore is not clear how the lapse time can be measured best. Quite obvious however is that each swarm phase resembles the behaviour of an aftershock sequence. To be able to find the parameters of the Omori formula, we put the lapse time origin into the onset of that sequence of each swarm phase which is defined by the latest well pronounced minimum of the waiting time curve. The K and p parameters were determined by a linear regression of a logarithmic version of (2); an optimal value of c was found by a grid search. The results (see Table 2 and Fig. 7) showed that a quite good correlation between τ and t is obtained for those relaxation periods, which are long enough and not disturbed by the occurrence of a secondary swarm sequence. The p values for these relaxation periods range from 0.95 to 1.26 which lies within the interval [0.7, 1.8] observed for aftershock sequences in California (Kisslinger and Jones, 1991) or [0.9, 1.4] for Japan (Guo and Ogata, 1997).

This finding indicates a partial similarity between the phases of the 2000 swarm and tectonically induced aftershocks for which the Omori law was derived. Hence we can infer that the stress redistribution and other mechanisms responsible for generating aftershock sequences are in some way present during the swarm generation process. However, the 2000 swarm probably is the first known NW-Bohemia/Vogtland swarm that displays this type of strong temporal clustering in the form of well-pronounced swarm phases (subswarms). Previous swarms in the same area, namely the large swarm of 1985/86 and the January 1997 swarm, exhibited a more chaotic picture of clustering in time, more different from the pattern typical for aftershock sequences (Horálek et al., 1987; Fischer and Horálek, 2000). Furthermore, in the course of the January 1997 swarm, crustal fluids are supposed to have played an active role with regard to the high value of isotropic components found in the moment tensors of a number of events (Horálek et al., 2000b).

4.2. Space-time distribution of the swarm

4.2.1. Shape of the focal area

The hypocentres of the 2000 swarm are shown in Fig. 8; displayed are only accurately located events ($S_0 < 6$) above the magnitude cutoff of 0.4. As follows from Fig. 8, the events were distributed on a steeply dipping, almost planar area of about 3×3 km size with an isolated, tail-shaped subcluster situated approximately 3 km to the north from the main cluster. The focal area dips steeply to the west; the dip is not uniform—it increases with depth, the bottom part dips almost vertically.

By comparing the epicentre view and the north-south cross section (see Fig. 8) it becomes clear that the main cluster may be subdivided into two almost parallel sections Part 1 and Part 2 which were active in different periods of the swarm activity (see below). The dividing plane denoted in the fig. dips approximately 50° to south. The depth range of the parts differ: while the bottom of both is strictly limited by 10.5 km depth, the depth of their top margin varies from 8.5 km at the northern Part 1 to 7.6 km at the southern Part 2.

Splitting of the main cluster into two distinct sections is also apparent from the distribution of stronger events ($M_L > 1.5$) in the east-west cross section (full circles in Fig. 8). These events form two branches within the bottom part of the focal area, each of them belonging to a different section of the main cluster. The left branch corresponds to the northern Part 1, while the right one is formed by events of the bottom of southern Part 2.

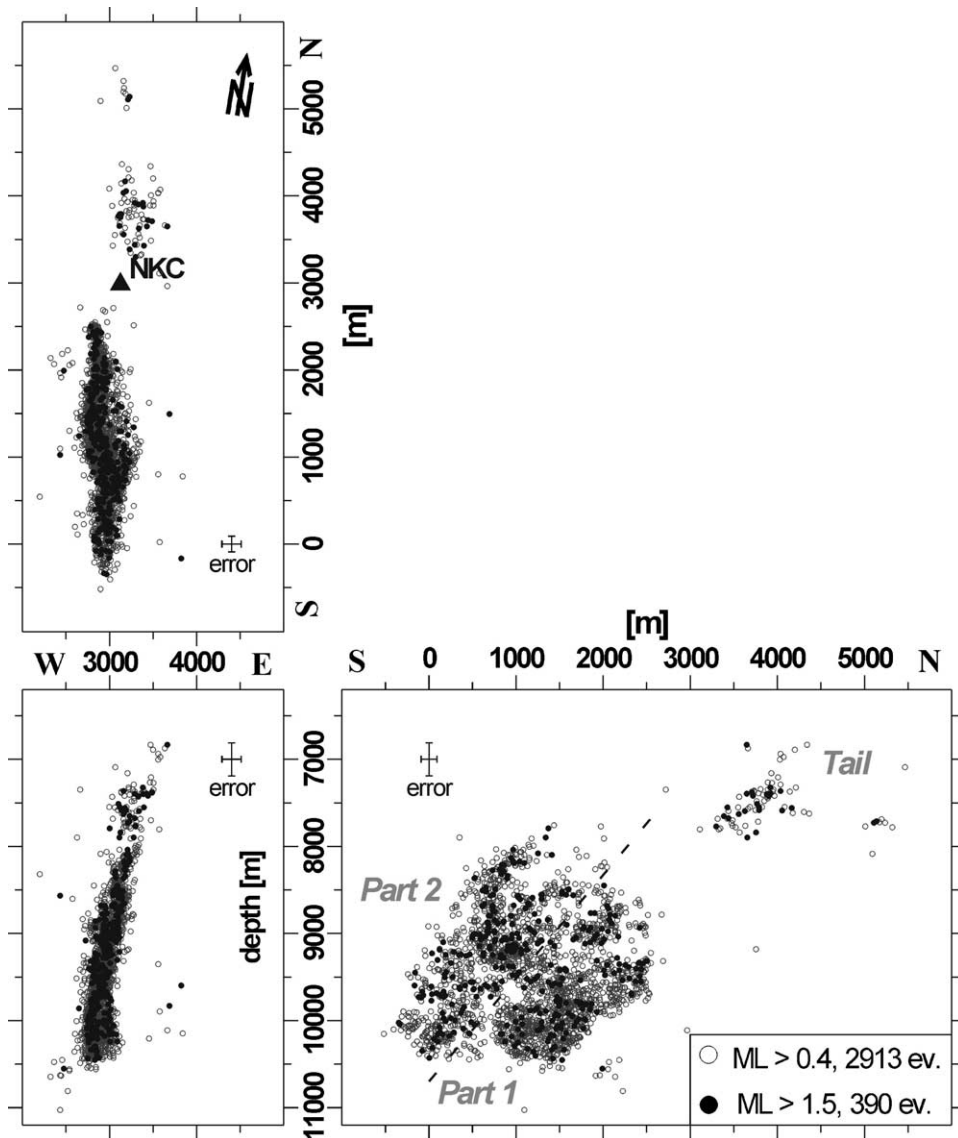


Fig. 8. Focal area of the swarm 2000. Top left—map view, bottom right—vertical cross section viewed from east, bottom left—vertical cross section viewed from south. The coordinate system is rotated 9° clockwise to east so that the focal area viewed from south has a minimum width. Only events with low location residuals S_0 are displayed. Error bars indicate typical relative location error. The main area is subdivided into subclusters Part 1 and Part 2, which were active during different periods. From the map view it seems that Part 1 and Part 2 are non-parallel, nevertheless comparing all three views indicates that the focal area is almost planar and the segmentation of the horizontal projection is an effect of different prevailing depth of the events within southern Part 2 and northern Part 1.

A complicated structure of the main cluster, formed by multiple subclusters isolated by zones without hypocentre occurrence, is apparent. The structure is even more pronounced at a higher magnitude level, see the hypocentres of $M_L > 1.5$ events in the north-south cross section in Fig. 8. Though the size of these zones is comparable to the location error, their existence looks real

because the effect of location error would result in a uniform scatter of hypocentres, hence no gaps would occur. To explain the origin of these gaps, the size of rupture areas of neighbouring events should be determined. If the rupture areas of adjacent events do not reach these zones, they remain unbroken and are either creeping, or behave like barriers which occur in parts of the fault surface with higher strength (Aki, 1979). Respectively oriented detailed studies unfortunately were not feasible within the scope of this paper because of the insufficient location accuracy of the automatic data processing procedure.

4.2.2. Migration of activity

Fig. 9 displays the distribution of hypocentres within particular swarm phases using two perpendicular vertical cross-sections. The figure shows that the foci of individual swarm phases occupied a limited volume. From the east-west cross-sections it follows that the hypocentres of each swarm phase were distributed close to a common fault plane, however the focal areas of some swarm phases were slightly declined from it.

A clear counter-clockwise migration of the activity is apparent: the swarm starts during the first phase P1 by a dense cluster at the bottom of Part 1. Then the hypocentres spread upwards and to north during the next two September phases P2 and P3. Within the last September phase P4 the activity dissipates along the whole northern Part 1; a concentration of the activity is observed at shallow depths near the axis of the whole swarm 2000 area. Some events also jumped into the southern Part 2. Then a long quiescence period, lasting 4 weeks, took place (see also Figs. 6 and 7). In mid October the uppermost cluster of the southern Part 2 was activated (P5). Later on the earthquakes migrated down - two weaker phases P6 and P7 took place in the centre of the whole swarm 2000 area. Also first events appeared at the northern Tail. During the November phase P8, which was the strongest one, the whole southern Part 2 was affected; the activity jumped also back to the bottom of the northern Part 1 where the swarm had started by its first phase in August. The whole swarm was terminated by the Christmas phase P9 taking place in the northern Tail. An isolated minor cluster appeared on Dec. 26 approximately 300 m NW and down from Part 1. This cluster is interesting by its anomalous position—unlike all other clusters, it is located apart from the common fault plane.

4.3. Estimating the fault plane solutions

4.3.1. First motion polarities and amplitudes

As an output of the automatic procedure, also the P- and SH- first motion polarities and amplitudes were obtained. The first motion amplitudes were automatically picked at the vertical component for P-waves and at the transversal component for SH-waves. The ground velocity records were first integrated and then high pass filtered by a causal 4th order Butterworth filter with a corner frequency of 0.3 Hz and 0.1 Hz for P- and S-waves, respectively. In view of the frequency content of the local events, the WEBNET seismograms are sufficiently broadband for local events with magnitudes between -0.5 and 4. To minimise the rate of incorrect readings, which are more frequent in the case of weak events, I used only events exceeding the magnitude of 0.9. The final data set consisted of amplitude and polarity data for 1242 events meeting the criteria for lower magnitude limit and location accuracy.

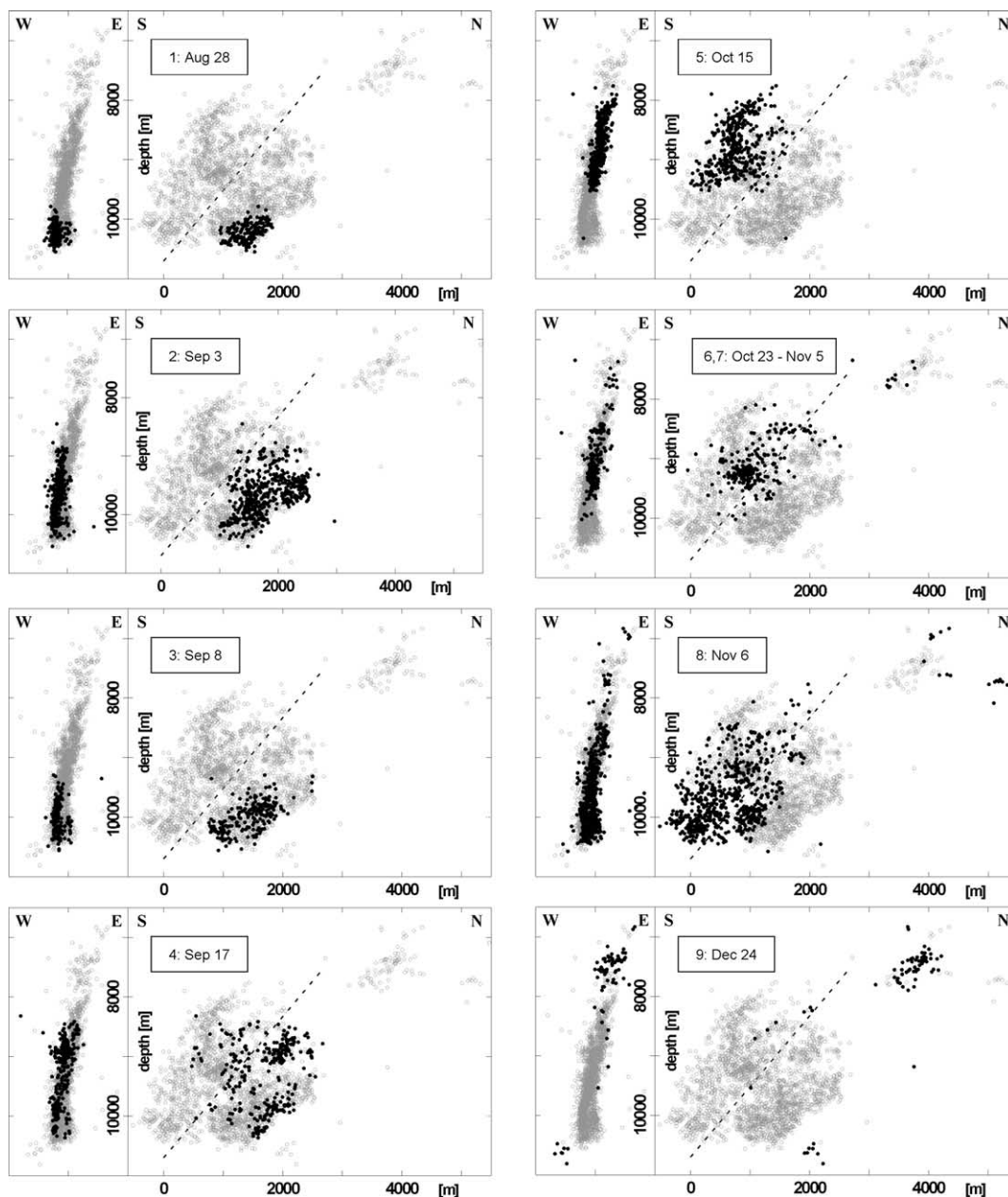


Fig. 9. Space–time distribution of the swarm 2000. Two vertical cross sections are used to display the relative position of each swarm phase. Left: view from south to north. Right: view from east to west. A counter-clockwise migration of activity is apparent.

First, the success rate of polarity picking was checked visually. The expected correctness of the P-wave first motion polarities was high, based on the results of testing the automatic method on the manually processed swarm of 1997, which occurred in the same focal area as the 2000 swarm. The comparison of automatic P-wave first motion polarities with those obtained manually

showed that 89% of them were correct (Fischer, 2002). In Fig. 10 the P- and SH-waveforms of all processed events are displayed for two selected stations. The plots show a remarkable similarity between the seismograms of individual events. This is not surprising—the swarm events usually occur as multiplets displaying identical waveforms and focal mechanism (Horálek et al., 2000a). The figure also indicates that the arrival time picks at KOC are more precise for P-waves than for S-waves and that several mistaken SH- polarity picks at NKC are caused by arrival time pick errors.

4.3.2. *P and T axes*

The first motion polarities and amplitudes of all the located events represent a valuable data set, which can help us study the temporal and spatial variation of focal mechanisms. In principle, the temporal variations of the first motion polarities and amplitude ratios would result from superposition of two effects: (1) migration of events on the fault plane and (2) temporal variations of focal mechanisms. In Fig. 11, the temporal dependence of the ratio $abs(A_{SH})/A_P$ is shown for each station to illustrate the absolute magnitude of the amplitude ratio and the onset polarity of P-wave. The figure shows an almost stable P-onset polarity and amplitude ratio at stations KRC and KOC, while at station LAC the P-onset polarity changed in the course of the swarm. An opposite situation occurred during the swarm 1997: P-onset polarities were absolutely monotonous at LAC, whereas the polarities at KRC and KOC changed in time what was the first indication of differing focal mechanisms of 1997 and 2000 swarms. The station NKC, situated just above the main cluster, shows a strong temporal variation of both P-onset polarity and amplitude ratio. To verify if these polarity changes are due to temporal variations of fault mechanisms, the effect of migration of events must be separated. For this purpose the fault plane solutions (FPS) were estimated and the resulting FPS were classified according to the type of faulting.

For FPS estimation, the FOCMEC program (Snoké et al., 1984) was used. Provided the takeoff angle error is negligible, and the earthquakes have a pure double-couple source, there should be full compliance between the theoretical and observed P- and SH-polarities, and any misfit should be due to the phase picking error of the automatic method. Because the wave azimuths were not well defined at the NKC station due to its position almost above the hypocentres, the SH-polarity was not used at NKC for the FPS estimation. Full compliance of the P-wave polarities was required and only one error in the SH-wave polarities was allowed. The other parameters of FOCMEC are summarised in Table 3. By refusing the events with unacceptable amplitude ratio misfit and rate of polarity errors, the FPS estimation also enabled me to check the correctness of the polarity and amplitude readings.

Depending on the angle step of the grid search, multiple acceptable solutions are usually found; as an optimal solution, that with the lowest misfit is chosen by FOCMEC. To be able to estimate also the uncertainty of the angles of the fault plane solution, which is not provided by FOCMEC, I used the P and T axes instead of the FPS angles (strike, dip, rake). As an optimal solution, the P and T axis corresponding to the vector sum of all acceptable P and T axes, respectively, was taken. Hence a mean value of P and T axis is obtained, while the error ϵ_P and ϵ_T of each axis corresponds to the angle size of the P and T axes cluster, respectively. In this way, the error expressing the numerical stability of each fault plane solution has been determined.

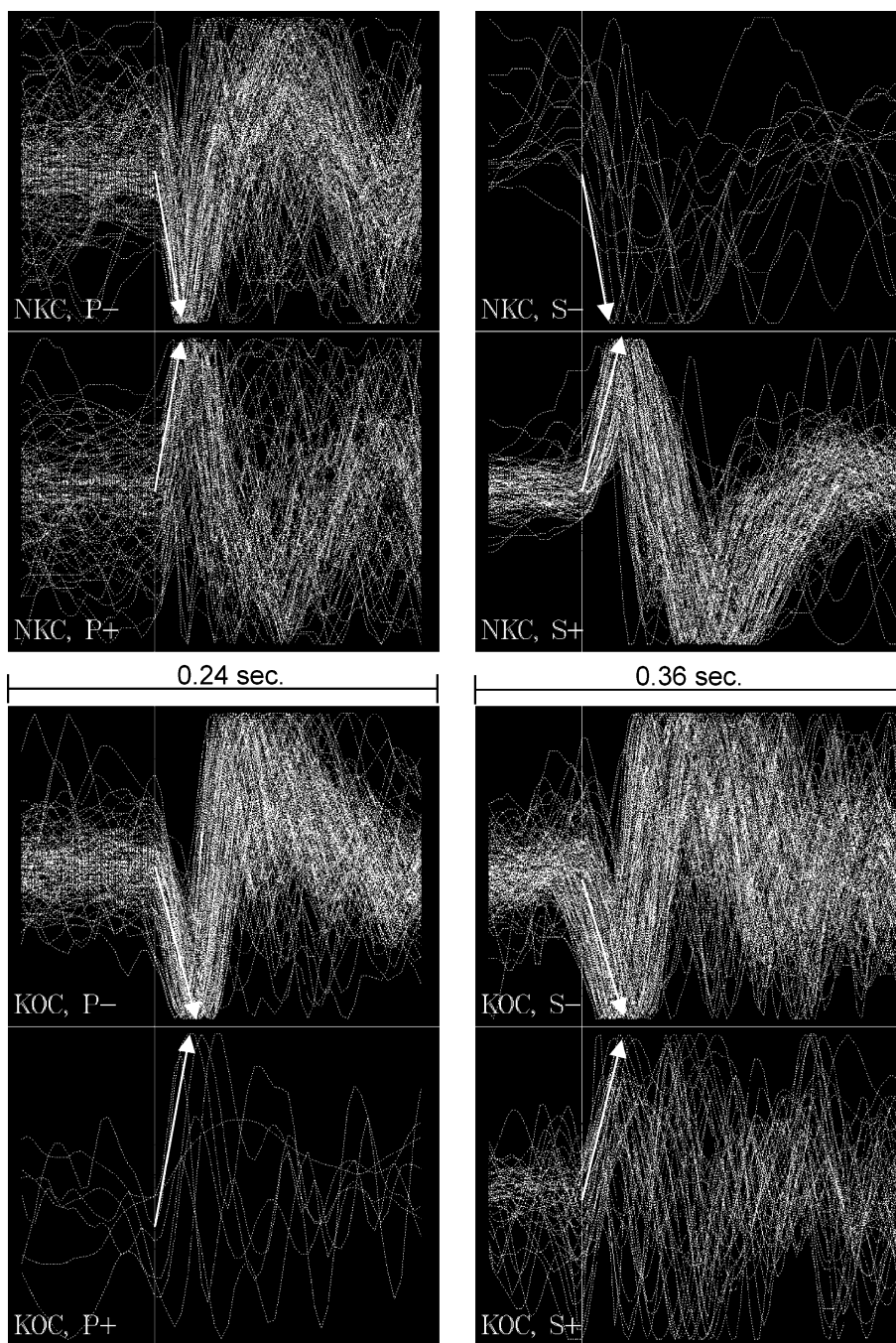


Fig. 10. P- and S-waveforms of the 1242 strongest events (criterion $M_L > 0.9$ and location residual $S_0 < 6$ samples). The integrated velocity records for the NKC and KOC stations are shown; vertical component for P- and transversal component for S-arrivals. The seismograms are aligned to a common, automatically picked arrival time and the opposite first motion polarities are displayed separately. The way of picking the onset amplitudes is indicated by arrows. The station code and the automatically assigned first motion polarity is printed in each plot. Note the stable S-waveform shape at both the stations in contrast to the varying P-waveform occurrence at NKC.

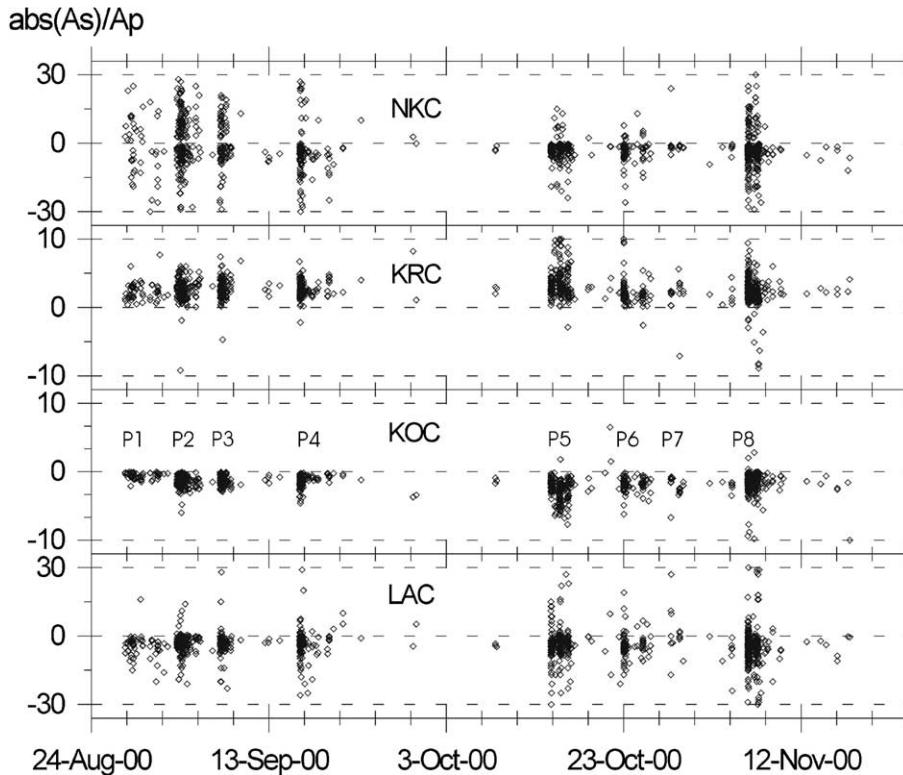


Fig. 11. Variation of amplitude ratios during the swarm. Note the varying absolute value of the A_S/A_P amplitude ratio at all stations in contrast to almost stable P-wave polarity at KOC.

Table 3
FOCMEC parameters

Angle step	Allowed errors			Lower limit for P and S radiation factor	Maximum allowed misfit of $\log(A_{SH}/A_P)$
	P-polarity	S-polarity	A_{SH}/A_P		
5°	0	1	0	0.01	0.6

For 1125 events at least one acceptable solution was found, 117 events did not pass the compatibility test of polarity and amplitude picks. To exclude ill-conditioned results, only events meeting the criterion $\text{SUM}(\epsilon_P + \epsilon_T) < 40^\circ$ were further processed. Hence, for altogether 782 events the P and T axes were obtained with an average error lower than 20° .

4.4. Classifying the events according to their faulting type

The distribution of the P and T axes of all 782 events (Fig. 12a) points to strong variations of focal mechanisms during the swarm 2000. Although the P axes show a wide range of plunge directions, most of them are almost vertical. In azimuths, the P axes maintain a general trend of

WWN-EES (azimuth 110°) orientation. In contrast, the T axes are almost horizontal and display a stronger clustering with the average azimuth of 200° . Based on the common assumption that the P and T axis represents the direction of maximum and minimum compressive stress we can conclude that the maximum compression axis was almost vertical, while the minimum compression axis showed subhorizontal NNE-SSW orientation. This indicates that the stress system governing the 2000 swarm was declined from the stress field obtained by previous studies, where a subhorizontal direction of both axes was found, with approximately SE-NW direction of the maximum compression and SW-NE direction of the minimum compression (Havíř, 2000; Wirth et al., 2000). This result however must be considered to be quite preliminary since the small number of stations available for the automatic processing may have brought a systematic shift to the fault plane solutions.

The prevailing near-vertical orientations of the P axes indicate that most of the events were of a normal faulting type; few events however show also T axes in a near-vertical direction pointing to their reverse character. To distinguish different faulting types the events were classified into the

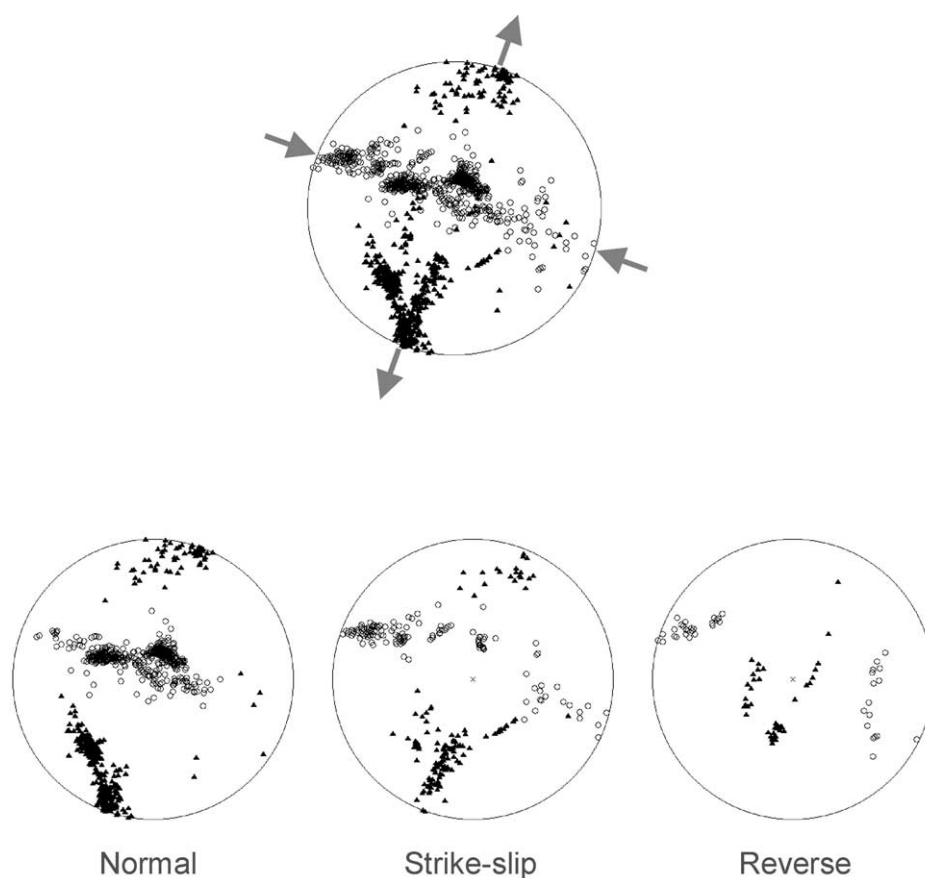


Fig. 12. (a) The distribution of P and T axes with an average error lower than 20° (782 events). Note a wide range of plunges of P -axes compared to well constrained T -axes. Arrows indicate the direction of maximum and minimum compression, corresponding to the trend of P - and T -axes clustering. (b) Three groups of events following their faulting type. A lower hemisphere, equal-area projection is used.

groups of normal, strike-slip and reverse events following the proximity of P and T axes to the vertical. For this purpose, the plunge φ and angle error ϵ of both axes was investigated and the event was declared as strike-slip if $abs(\varphi_P - \varphi_T) < \epsilon_P + \epsilon_T$. The remaining events were classified according to the φ_P to φ_T interrelation: $\varphi_P < \varphi_T$ for normal events, $\varphi_P > \varphi_T$ for reverse events. The resulting groups of the P and T axes are illustrated in Fig. 12b. As expected, the normal and strike-slip events were the most frequent and also the strongest ones: they comprised 95% of all investigated earthquakes. Their energetic contribution was even much higher—all the $M_L > 2.0$ earthquakes were of normal and strike-slip type.

It is noteworthy to emphasise that the FPS classification was carried out with the main aim to find similar features of the swarm events and in order to provide a first, approximate classification. Presumably the results should help draw first characteristics of swarm phases and clusters and select the events for the further detailed focal mechanism studies.

The space and time distribution of the different event types is shown in Fig. 13. The fig. indicates that the space-time distribution of the earthquake hypocentres differs essentially: the normal events are distributed almost uniformly along the whole fault plane, whereas the strike-slip events appear in the whole Part 1 and in the bottom of Part 2 of the main cluster. Seldom reverse events form two dense clusters and are scattered in the bottom part of the main cluster. Another interesting feature of space clustering of the reverse events is apparent in the East-West cross section: their hypocentres in the bottom part appear along an isolated, steeply dipping plane, the dip of which is opposite to the dip of the whole focal area formed by normal and strike-slip events. In other words, the whole focal area dips to the west, whereas the cluster of reverse events dips to the east. This can explain the reverse faulting of these events: the same stress tensor may generate different slips on fault planes of different orientation. A similar situation has been described Dahm et al. (2000) and Horálek et al. (2000b) for the events of the swarm of 1997 that occurred in the same focal area.

The temporal occurrence of various faulting types reflects their space distribution and the migration of the events. As follows from the bottom plot of Fig. 13, in contrast to normal events occurring during the whole swarm duration, strike-slip and reverse events were typical for specific swarm phases. While the reverse events took place prevalingly within swarm phases P2 and P8, the strike-slip events occurred more frequently, but were almost missing during the phases P3, P5, P6, and P7.

5. Conclusions

The NW Bohemian earthquake swarm of 2000 has been investigated using an advanced method of automatic processing of local seismic network seismograms (Fischer, 2002). The automatic method made it possible to process the local multistation data rapidly and objectively. Results upon the spatial extent, the magnitude range, the space-time distribution of the whole swarm, and a basic classification of the events according to their focal mechanisms were available shortly after the occurrence of the swarm.

The swarm occurred in August – December 2000 in the Nový Kostel focal area. The data from the four most sensitive stations of the local seismic network WEBNET were treated. Altogether 7017 earthquakes in the magnitude range from 0 to 3.3 occurring in the Nový Kostel focal area

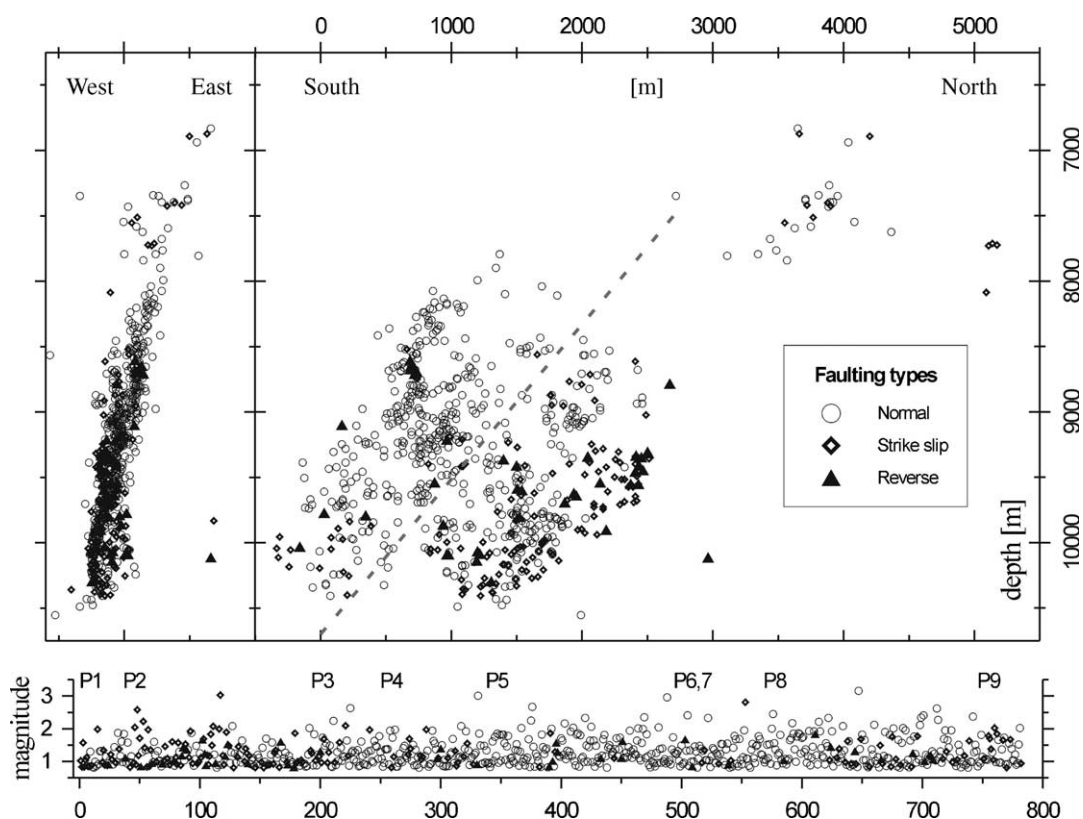


Fig. 13. Space–time distribution of events of different faulting types. Top left: vertical cross section viewed from east. Top right: vertical cross section viewed from south. Bottom: magnitude–time occurrence of faulting types. Note the clear clustering of the reverse faulting types, both in space and time. P1–9 indicate the swarm phase numbers.

were identified. The resulting seismic catalogue is considered to be complete down to the local magnitude of 0.4. It comprises 1385 $M_L > 1.0$, 131 $M_L > 2.0$ and eight $M_L > 3.0$ events. The swarm 2000 displayed a strongly episodic character—nine swarm phases isolated by quiescence periods were distinguished. The maximum magnitudes of each of the swarm phases exceeded the value of 2.5, whereas during the quiescence periods only $M_L < 1.0$ events appeared. Investigation of the inter-event time distribution revealed that during the relaxation periods of the swarm phases the waiting times followed the modified Omori law with P -values in-between 0.95 and 1.26.

The hypocentres of the swarm events were distributed along a north-south oriented, almost circular, steeply dipping fault area of a 3 km diameter with a linear appendix pointing to the north. Their space-time distribution exhibits a pronounced bottom \Rightarrow top \Rightarrow bottom and north \Rightarrow south migration.

Fault plane solutions of the 782 strongest events were estimated by the FOCMEC program. The orientation of the P - and T -axes indicates that the local stress field was declined by 40° counter-clockwise from the regional one. The swarm was dominated by normal and strike-slip events with M_L magnitudes of up to 3.3. Much weaker reverse events not exceeding M_L of 2.0

took place rarely in the first swarm period and in the strongest November phase. The reverse events markedly clustered in space and occurred probably on minor fault planes, which were slightly declined from the main fault plane.

Acknowledgements

Fruitful and stimulating discussions with A. Boušková and J. Horálek are greatly appreciated. The author wishes to thank A. Plešinger for careful reading the manuscript and tips for enhancing the text. The work also earned significantly from the stimulating suggestions of the reviewers T. Dahm and M. Jost. This research was carried out under GA CR Grant Project No. 205/99/0907 “Recent Geodynamics of West Bohemia in Relation to the Crustal Structure (Unique Natural Laboratory)”.

References

- Aki, K., 1979. Characterizations of barriers on an earthquake fault. *J. Geophys. Res.* 84, 6140–6148.
- Antonini, M., 1988. Variations in the focal mechanisms during the 1985/86 Western Bohemian earthquake swarm sequence—correlation with spatial distribution of foci and suggested geometry of faulting. In: Procházková, D. (Ed.), *Induced Seismicity and Associated Phenomena*. Geophys. Inst. of Czechosl. Acad. Sci, Praha, pp. 250–270.
- Boušková, A., Hudová, Z., Kratochvíl, P., 2002. Personal communication.
- Čermák, V., Šafanda, J., Krešl, M., Kučerová, L., 1996. Heat flow studies in Central Europe with special emphasis on data from former Czechoslovakia. *Global Tect. Metallogeny* 5, 3. /4, 109–123.
- Dahm, T., Horálek, J., Šílený, J. Comparison of moment tensor solutions for the January 1997 West Bohemia earthquake swarm. *Studia Geoph. et Geod* 44, 233–250.
- Dudek, A., 1987. Geology and tectonic pattern of the Western Bohemia seismic area. In: Procházková, D. (Ed.), *Earthquake Swarm 1985/86 in Western Bohemia*. Geophys. Inst. Czechosl. Acad. Sci., Praha, pp. 34–37.
- Fischer, T., Horálek, J., 2000. Refined locations of the swarm earthquakes in the Nový Kostel focal zone and spatial distribution of the January 1997 swarm in Western Bohemia, Czech Republic. *Studia Geoph. Geod* 44, 210–226.
- Fischer, T., 2002. Automatic processing of local swarm microearthquakes: a location—controlled method applied on WEBNET. *Studia Geoph. et Geod.* (submitted for publication).
- Grosser, H., Burghardt, P.Th., Kohler, W., 1987. Spectral calculations and focal parameter studies of selected events of the West Bohemia earthquake swarm 1985/1986. In: Procházková, D. (Ed.), *Induced Seismicity and Associated Phenomena*. Geophys. Inst. of Czechosl. Acad. Sci, Praha, pp. 282–291.
- Guo, Z., Ogata, Y., 1997. Statistical relations between the parameters of aftershocks in time, space and magnitude. *J. Geophys. Res.* 102 (B2), 2857–2873.
- Hainzl, S., Zoeller, G., Kurths, J., 2000. Self-organization of spatio-temporal earthquake clusters. *Nonlinear Processes in Geophysics* 7, 21–29.
- Hainzl, S., 2002. Self-organization of earthquake swarms. *J. Geodynamics* (this issue).
- Havíř, J., 2000. Stress analyses in the epicentral area of Nový Kostel (Western Bohemia). *Studia Geoph. Geod* 44, 522–536.
- Hill, D.P., 1977. A model for earthquake swarms. *J. Geophys. Res.* 82 (8), 1347–1352.
- Heinicke, J., 2000. Koch, U, Slug flow—a possible explanation for hydrogeochemical earthquake precursors at Bad Brandbach, Germany. *Pure Appl. Geophys* 157, 1621–1641.
- Horálek, J., Vavryčuk, V., Plešinger, A., Pšenčík, I., Jedlička, P., Soukup, J., 1987. Refined localizations of the Jan. 5–Feb. 6, 1986 events of the West-Bohemian earthquake swarm. In: Procházková, D. (Ed.), *Earthquake Swarm 1985/86 in Western Bohemia*. Geophys. Inst. of Czechosl. Acad. Sci, Praha, pp. 226–235.

- Horálek, J., Fischer, T., Boušková, A., Jedlička, P., 2000a. Western Bohemia/Vogtland region in the light of the WEBNET network. *Studia Geoph. Geod* 44, 107–125.
- Horálek, J., Šílený, J., Fischer, T., Slancová, A., Boušková, A. Scenario of the January 1997 West Bohemia Earthquake swarm. *Studia Geoph. Geod* 44, 491–521.
- Janský, J., Horálek, J., Málek, J., Boušková, A., 2000. Homogeneous velocity models of the West Bohemian swarm region obtained by grid search. *Studia Geoph. Geod* 44, 158–174.
- Jost, M.L., Büsselberg, T., Jost, Ö., Harjes, H.-P., 1998. Source parameters of injection-induced microearthquakes at 9 km depth at the KTB DeepDrilling Site, Germany. *Bull. Seism. Soc. Am.* 88, 815–832.
- Kagan, Y.Y., Jackson, D.D., 1991. Long-term earthquake clustering. *Geophys. J. Int* 104, 117–133.
- Kisslinger, C., Jones, L.M., 1991. Properties of aftershock sequences in Southern California. *J. Geophys. Res.* 96 (B7), 11947–11958.
- Lay, T., Wallace, T.C., 1995. *Modern Global Seismology*. Academic Press, New York.
- Magotra, N., Ahmed, N., Chael, E., 1987. Seismic events detection and source location using single-station (three-component) data. *Bull. Seism. Soc. Am* 77, 958–971.
- Mrlina, J., 2000. Vertical displacement in the Nový Kostel seismoactive area. *Studia Geoph. Geod* 44, 336–345.
- Neunhöfer, H., 2000. The Catalogue of the Vogtland/Western Bohemia Earthquakes and Vocatus as an Auxiliary Code. *Studia Geoph. Geod* 44, 549–555.
- Snoke, J.A., Munsey, J.W., Teague, A.G., Bollinger, G.A., 1984. A program for focal mechanism determination by combined use of polarity and SV/P amplitude ratio data. *Earthquake Notes* 55(3) 15.
- Šílený, J., 1987. Quasi-tomographic single event localization of Western Bohemia swarm events by means of local stations. In: Procházková, D. (Ed.), *Earthquake Swarm 1985/86 in Western Bohemia*. Geophys. Inst. of Czechosl. Acad. Sci, Praha, pp. 218–225.
- Špičáková, L., Uliěný, D., Koudelková, G., 2000. Tectonosedimentary evolution of the Cheb Basin (NW Bohemia, Czech Republic) between the Late Oligocene and Pliocene: a preliminary note. *Studia Geoph. Geod* 44, 556–580.
- Švancara, J., Gnojek, I., Hubatka, F., Dědáček, K., 2000. Geophysical field pattern in the West Bohemian geodynamic active area. *Studia Geoph. Geod* 44, 307–326.
- Utsu, T., 1961. A statistical study on the occurrence of aftershocks. *Geophys. Mag* 30, 521–605.
- Vavryčuk, V., 2001. Inversion for parameters of tensile earthquakes. *Tectonophysics* 336, 151–161.
- Wagner G. A., Gögen K., Jonckheere R., Kämpf H., Wagner I., Woda C., 1998. The age of Quaternary volcanoes Železná Hůrka and Komorní Hůrka (Western Eger Rift), Czech Republic: alpha-recoil track, TL, ESR and fission track chronometry. In: *Magma and Rift Basin Evolution—Excursion Guide, Abstracts, Czech Rep., Liblice, 7–11 Sept., 1998*. Czech Geol. Survey, Prague, pp. 95–96.
- Weise, S., Brauer, K., Kampf, H., Strauch, G., Koch, U., 2001. Transport of mantle volatiles through the crust traced by seismically released fluids: a natural experiment in the earthquake swarm area Vogtland/NW Bohemia, Central Europe. *Tectonophysics* 336, 137–150.
- Wirth, W., Plenefisch, T., Klinge, K., Stammler, K., 2000. Focal mechanisms and stress field in the region Vogtland/Western Bohemia. *Studia Geoph. Geod* 44, 126–141.
- Yamashita, T., 1999. Pore creation due to fault slip in a fluid-permeated fault zone and its effect on seismicity: generation mechanism of earthquake swarm. *Pure Appl. Geophys* 155, 625–647.
- Zahradník, J., Janský, J., Vavryčuk, V., Zedník, J., 1989. Focal mechanisms of selected events of the West-Bohemia earthquake swarm 1985/86 constrained by P-wave amplitudes. *Rev. de Geofisica* 45, 217–230.